Effects of clogging on ultrasonic transmission through saturated granular single and double porosity media

Fatima Zahraa Kachkouch, Abdellah Alem, Alain Tinel, Hervé Franklin, Huaqing Wang

Version of Record: https://www.sciencedirect.com/science/article/pii/S0041624X20301402
Manuscript_906ac31c7bd1e5a5e61e133a0c0724c2

Effects of clogging on ultrasonic transmission through saturated granular single and double porosity media

Fatima Zahraa Kachkouch, Abdellah Alem, Alain Tinel, Hervé Franklin, Huaqing Wang

Laboratoire Ondes et Milieux Complexes UMR CNRS 6294

Université Le Havre Normandie 75, rue Bellot 76600 Le Havre France

Abstract

The clogging caused by the deposition of suspended particles modifies in depth several mechanical parameters (permeability, porosity, bulk moduli, etc.) of porous media and influences the acoustic behaviour. Consequently, at a fixed position in the medium, changes in phase velocity and attenuation are observed in the amplitude of the temporal signal of the transmitted waves. In this work, ultrasonic techniques are presented both for detecting and measuring the clogging in a water saturated porous medium. The acoustic measurements from the clogged samples are compared with the deposition profiles obtained at the end of injection experiments. Moreover, links are established between on the one hand phase velocity and the total porosity, and on the other hand the transmitted signal energy and the variation of porosity as consequence of particle deposition.

Keywords: clogging, granular media, single porosity, double porosity, acoustic waves

1. Introduction

During the flow of suspended fine particles through single or double porosity poroelastic media (referred to hereafter by SPP and DPP), several phenomena are likely to occur, causing adverse consequences on the proper functioning of the structures. It has been shown that the clogging of recovery wells is due to the presence of fine particles in the water [1]. The decrease in permeability [2], one of the consequences resulting from the clogging, can affect the proper functioning of the structure. Conversely, the detachment of particles and their transport by water flow can provoke internal erosion. This phenomenon is hardly detectable in its first manifestations.

The paper presents a nondestructive ultrasonic method for detecting the accumulation of deposited particles in SPP and DPP. The acoustic properties of the porous material must be related to the mechanical parameters. In the case of clean media (not crossed by a turbid flow), Kohout *et al*. [3] showed that the propagation velocities of acoustic waves depend on the porosity of the material. Based on the velocity of the slow longitudinal wave, tortuosity was determined at high frequency [4-5], and permeability at low frequency [6].

The coupling between a destructive method discussed later in the paper and the ultrasonic method requires at first understanding how the acoustic waves propagate through such complex media. The model describing acoustic wave propagation in fluid saturated SPP media is due to Biot [7]. The travelling of waves through poroelastic slabs allows extracting certain poroelastic parameters [8]. Lauriks *et al*. [9] have developed techniques for determining the physical parameters and elastic properties of the porous medium at high-frequency domain.

The majority of the aforementioned studies on acoustic wave propagation and/or fine particle filtration focused exclusively on SPP media. However, porous structures present in nature, contain fractures (macroporosity) and a finer porosity in the matrix (microporosity). This is why Biot's SPP model was extended to the case of a DPP medium [10-12]. From this later model, recent studies on double porosity were led. Dai et al. [13] studied reflection and transmission coefficients at a fluid-DPP interface. Kachkouch et al. [14] studied the dispersion curves of a double porosity plate. Using the transmission coefficient, frame bulk and shear moduli of double porosity media were estimated [15]. Note that other approaches ignored here [16, 17], derived alternative equations for DPP media from homogenization methods.

Our study considers both the theory of Biot (for the non-porous glass beads based medium) and of Berryman and Wang (for the porous grains based medium). The acoustic behavior in such materials strongly depends on the interaction between the two phases which have very different porosities, and on the friction between contacting grains [18]. For longitudinal waves, Kimura [19] developed a model showing that Biot's theory remains valid until $k_0 b < 0.5$ (k_0 is the wave number in water and b the diameter of the grains). That means working at low frequencies domain where it is known that the wavelengths involved are much greater than the characteristic pore sizes, and where it is also known that the nonlinear effects resulting from the friction between the grains can be neglected. In our case, considering a granular medium with a diameter of grains close to 3.5 mm and pores sizes detailed in section 2.1, means working at a frequency range around 40 kHz. Thus, the use of transducers with 44 kHz central frequency as we do in this paper means that we accept the measurements obtained as valid in the context of continuous media. Beyond approximately this frequency range, the effects of multiple scattering should also be considered.

To carry out the experiments, an elongated rectangular column intended to contain the porous materials was manufactured. Since clogging does not manifest in the same way along the column - it is more important at the entrance and decreases with depth - the experimental set up developed by Bai *et al*. [20] has been improved: (i) by changing the disposition of the column from vertical to horizontal, implying an horizontal flow which better corresponds to the flow occurring in water retention structures, see Fig. 2, (ii) by allowing a translation of the transducers along the column (from the inlet to the outlet of the flow). Notice that gravity may be a more significant force for particle deposition for horizontal flow than for down flow as it has been shown in previous research (Chrysikopoulos *et al*. [21]).

In section 2, the three materials used in this paper and the equations governing the acoustic wave propagation in SPP and DPP media are recalled. The experimental setup combining the destructive method and the ultrasonic measurements is then described. Section 3 is devoted to the equations of particle filtration and to the results of the destructive injection method. A follow-up of clogging in space (deposition profiles) and in time (restitution curves) is achieved. Section 4 is concerned with the results of ultrasonic detection of deposition. The velocities of the fastest longitudinal wave are estimated at first for the clean medium and next during injection. Comparison with the theoretical values is led for the clean medium only. The variation of the

signal energy and attenuation are represented based on the decrease of the transmitted signal amplitude. Finally, section 5 confronts the two methods and allows establishing links between phase velocities and the total porosity at the end of the injection process on the one hand, and between energy and the porosity variation due to deposition on the other hand.

2. Background on porous media

2.1. Description of samples

The SPP medium (also referred to as GB) is formed by stacking spherical glass beads of diameter 3.5 mm. The random arrangement of the beads creates empty spaces called pores which will be filled with water. Also, two kinds of DPP media are investigated. The first - Tobermorite - is a stack of porous grains of semi-natural material Tobermorite 11 Å (porous cement grains irregularly shaped and sized from 3.15 mm to 4 mm obtained by sieving) (Figs. 1c, 1d). The second - Robu - is a stack of porous grains of Borosilicate glass (VitraPOR® Sinterfilter & Laboratory Glassware) (Figs. 1a, 1b). This latter is widely used in research field because of its resistance to heat, corrosion and thermal shock. Robu and Tobermorite present a dual porosity: macroporosity between the grains and microporosity inside the grains. The total porosities of the three samples measured using air pycnometer D5550-6 are 39%, 60% and 70% for GB, Robu and Tobermorite, respectively. Porosity and pore size distributions in the grains were determined with mercury intrusion porosimetry. Microporosity is 21% of the total volume for Robu, and 31% of the total volume for Tobermorite. For Robu pore sizes ranged between 6 μm and 147 μm with h_{10} = 39 μm, h_{50} = 54 μm and h_{90} = 100 μm and for Tobermorite between 0.08 μm and 100 μm with h_{10}=0.06 μm, h_{50}=1.35 μm and h_{90}=14 μm (h_{10}, h_{50} and h_{90} are pore diameters corresponding respectively to 10%, 50% and 90% of the cumulative pore size distribution). Measurements allow to estimate a macroporosity of 39% of the total volume both for Robu and Tobermorite.

Several physical parameters characterize each of the materials described above (the numerical values are taken, for Glass beads from Kimura [22], and for the two DPP media from Bai *et al.* [20]). Most of these parameters are interdependent. For example, permeability is one of the most important parameters in a porous medium and is directly related to the size of the grains [3] and to the porosities.

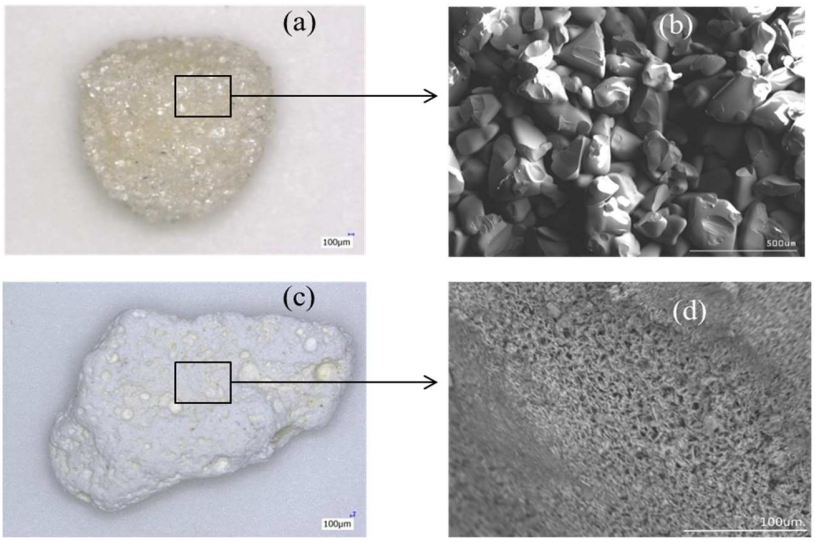

Fig. 1. (a) A grain of Robu (size is 3.5 mm), (b) view at MEB. (c) A grain of Tobermorite 11 Å (grain size can vary from 3.15 mm to 4 mm), (d) view at MEB.

2.2. Poroelastic waves

2.2.1. Biot's theory for a SPP medium

The porous medium is made up of two separately connected phases, the elastic matrix (skeleton) and the fluid that occupies the pore space. Let us introduce ρ_f the mass density of fluid, η the fluid viscosity, ρ_s the mass density of the elastic constituent, ϕ the porosity and k the permeability of the skeletal frame. The mass density of the porous medium is $\rho=(1-\phi)\rho_s+\phi\rho_f$. Let $\boldsymbol{u}$, $\boldsymbol{U}$ and $\boldsymbol{w}=\phi(\boldsymbol{U}-\boldsymbol{u})$ be the solid displacement, the pore fluid displacement and the relative fluid to solid displacement vectors, respectively. The constitutive equations for a porous saturated isotropic medium are

$$\overline{\overline{\tau}}=\left[(H-2\mu)\varepsilon_I+C\xi\right]\overline{\overline{I}}+2\mu\overline{\overline{\varepsilon}}, \tag{1}$$

$$P_f=-C\varepsilon_I+M\xi, \tag{2}$$

where $\overline{\overline{\tau}}$ is the stress tensor, P_f the fluid pressure, $\overline{\overline{\varepsilon}}=\left(\nabla\boldsymbol{u}+\nabla\boldsymbol{u}^T\right)/2$ the strain tensor (∇ is the gradient operator), $\overline{\overline{I}}$ the unit tensor, $\xi=-\nabla.\boldsymbol{w}$ the increment of fluid content and $\varepsilon_I=tr(\overline{\overline{\varepsilon}})=\nabla.\boldsymbol{u}$

the dilatation of the volume element attached to the frame. The constants μ, H, M and C represent poroelastic moduli (Stoll *et al*. [23]).

Wave equations for longitudinal and transverse waves were derived by Biot [7] from the constitutive equations, the equations of flow through a porous medium and the equations of motion. Let us assume fields harmonic in space and time ($e^{i(\ell x-\omega t)}$ dependence with propagation along the horizontal x axis) where ω is the angular frequency, t the time and $\ell=\ell_r+i\ell_i$ a complex wave number - ω/ℓ_r is the phase velocity and $2\pi\times 8.686\times\ell_i/\ell_r$ the attenuation coefficient. The dispersion relations are given by:

$$\begin{vmatrix} H\ell^2-\rho\omega^2 & \rho_f\omega^2-C\ell^2 \\ C\ell^2-\rho_f\omega^2 & m\omega^2-M\ell^2-i\omega\eta F/k \end{vmatrix}=0 \tag{3}$$

for longitudinal waves, and

$$\begin{vmatrix} \mu\ell^2-\rho\omega^2 & \rho_f\omega^2 \\ -\rho_f\omega^2 & m\omega^2-i\omega\eta F/k \end{vmatrix}=0 \tag{4}$$

for transverse waves [23]. Above, $m=a\left(\rho_f/\phi\right)$ where a (≥ 1) represents the structure factor accounting for the apparent increase in fluid inertia caused by the tortuosity of the pores. The Biot complex correction factor $F=F(\chi)$ and $\chi=a_p\left(\omega\rho_f/\eta\right)^{1/2}$ (where a_p is the pore size parameter) accounts for the fact that at higher frequencies, the fluid flow in the pores no longer respects the Poiseuille type flow. At low frequency, $F(\chi)=1$ and therefore disappears from the equations. Eq. (3) has two roots: one corresponds to the fast wave having moderate attenuations; the other to slow wave with strong attenuations (the existence of which was proved in Plona experiments [24]). Eq. (4) has a unique root. Longitudinal and transverse waves are decoupled.

2.2.2. Berryman and Wang extension of Biot's theory to DPP medium

In the equations of motion for fluid-saturated DPP media [12], $\boldsymbol{u}$, $\boldsymbol{U}^{(1)}$ and $\boldsymbol{U}^{(2)}$ denote the displacement vector of the solid frame, the micropore fluid (phase 1) and the macropore fluid (phase 2), respectively. The relative fluid-solid displacements are $\boldsymbol{w}^{(j)}=\nu^{(j)}\phi^{(j)}\left(\boldsymbol{U}^{(j)}-\boldsymbol{u}\right)$, in micropores ($j=1$) and in macropores ($j=2$). The coefficient $\phi^{(1)}$ ($\phi^{(2)}$) is the volume fraction of micropores in matrix (of fracture porosity) with $\phi^{(2)}=1$; $\nu^{(1)}$ ($\nu^{(2)}$) is the volume fraction

occupied by matrix (by macropores) with $\sum_j \nu^{(j)} = 1$, so that $\nu^{(1)}\phi^{(1)}$ represents the volume fraction of micropores in the medium. The increments of fluid content are defined by $\xi^{(j)} = -\nabla.\boldsymbol{w}^{(j)}$. Let $\overline{\overline{\tau}}$ be the stress tensor and $P^{(j)}$ ($j = 1, 2$) be the fluid pressures. The constitutive relations for isotropic DPP media are

$$\overline{\overline{\tau}} = \left[\left(H - 2\mu \right) \varepsilon_I - C^{(1)} \xi^{(1)} - C^{(2)} \xi^{(2)} \right] \overline{\overline{I}} + 2\mu \overline{\overline{\varepsilon}}, \tag{5}$$

$$\begin{pmatrix} P^{(1)} \\ P^{(2)} \end{pmatrix} = \begin{pmatrix} -C_{12} & C_{22} & C_{23} \\ -C_{13} & C_{23} & C_{33} \end{pmatrix} \begin{pmatrix} \varepsilon_I \\ \xi^{(1)} \\ \xi^{(2)} \end{pmatrix}. \tag{6}$$

The strain tensor $\overline{\overline{\varepsilon}}$ and its trace ε_I have been defined above, in sec. 2.2.1. In Eq. (5)

$$H = K_u + \frac{4}{3}\mu + \nu^{(1)}\phi^{(1)}C_{12} + \nu^{(2)}C_{13}, \tag{7}$$

$$C^{(1)} = -K_u B^{(1)} + \nu^{(1)}\phi^{(1)}C_{22} + \nu^{(2)}C_{23}, \tag{8}$$

$$C^{(2)} = -K_u B^{(2)} + \nu^{(1)}\phi^{(1)}C_{23} + \nu^{(2)}C_{33}. \tag{9}$$

where μ and K_u represent the shear modulus for the skeletal frame and the undrained bulk modulus of the DPP medium, respectively. Note that K_u depends on Skempton's pore-pressure build-up coefficients $B^{(j)}$ ($j = 1, 2$) [12]. The constants H, $C^{(1)}$ and $C^{(2)}$ define moduli for the DPP medium considered as a continuum. More details on the way to compute the coefficients $B^{(j)}$ and C_{ij} ($C_{ij} = C_{ji}$ with a dependence on the moduli K_u, K_1, K_2, K, K_s, $K_s^{(1)}$, μ given in Table 1 of Ref. [20]) can be found in the paper of Dai *et al.* [25] with the C_{ij}s corresponding to their A_{ij}s. Eqs. (7-9) represent the constitutive equations of isotropic DPP media.

Following the same method as in sec. 2.2.1, wave equations for longitudinal and transverse waves were derived by Berryman and Wang [12] from the constitutive equations, the equations of motion and the equations of flow through a DPP medium. Assuming once again fields with a $e^{i(\ell x - \omega t)}$ dependence, the dispersion relation can be written as

$$\begin{vmatrix} t_{11} & t_{12} & t_{13} \\ t_{21} & t_{22} & t_{23} \\ t_{31} & t_{32} & t_{33} \end{vmatrix} = 0 \tag{10}$$

for longitudinal waves and

$$\begin{vmatrix} q_{11} & q_{12} & q_{13} \\ q_{21} & q_{22} & q_{23} \\ q_{31} & q_{32} & q_{33} \end{vmatrix} = 0 \tag{11}$$

for transverse waves. The elements t_{ij} and q_{ij} of the determinants are given in the Appendix. They differ from that given by Dai *et al*. [25] or Berrryman and Wang [12]. The latters observed the presence of an additional longitudinal wave due to the presence of a second network of connected pores (micropores inside the grains). The theoretical proofs are not reproduced here; however, in sec. 4, we compute the phase velocities using the values of Table 1 of Ref. [20] and compare them with the experimental measurements.

2.3. Experimental setup

The first equipment allows for acoustic measurements, the second allows the estimation of particle retention in order to evaluate the clogging. The porous material (either SPP or DPP medium) is set in an aluminum rectangular column of dimensions 100 x 100 x 450 mm^3 (wall thickness is 2 mm). The column is placed horizontally to avoid any settling causing heterogeneity of the material and is fully immersed in a large water-filled tank for at least 24 hours so that the porous media are totally saturated. To perform ultrasonic measurements, the two immersion transducers (Ultran group GC50-D50) - Ø5 cm and central frequency 44 kHz - positioned opposite each other (without contact with the metal plates) were used. Using a mechanical translation system that maintains fixed the distance from the column, these transducers (one acting as the emitter of acoustic waves, the other as the receiver) can move along the horizontal axis (Fig. 2) (eight different positions are defined for the results).

A generator (Sofranel model 5058 PR) delivers pulses of amplitude 300V and duration 200ns; the oscilloscope synchronization signal is also delivered by the generator. The received signals are digitized, averaged over 200 acquisitions by a Lecroy 9310 AL digital oscilloscope (400 MHz bandwidth) and then stored on a computer linked to the oscilloscope.

The column was fed by reservoir containing water (pH of 6.7 ± 0.2) and suspended particles (SusP) (Portland kaolinite particles with average diameter of 11 µm) using a Cole-Parmer Master flex peristaltic pump with flow rate control. The suspension is injected through the porous medium over a longer time at constant flow. Six piezometers are placed on the column as indicated in Fig. 2 to measure the pore pressure variation along the porous medium. At the outlet of the column, the effluent was passed through a continuous flow turbidimeter (Kobold Instruments) to record the turbidity values in terms of Nephelometric Turbidity Units (NTUs). Suspended particles concentrations in the effluent, noted C, were determined with the help of correlations made between measured suspended particles concentrations in the water and values in NTU given by the turbidimeter. The SusP injection experiments were conducted with a constant injection concentration $C_0 = 1 g / l$ and flow velocity of 0.013 cm.s^{-1}. At the end of each experiment, the material (porous medium with deposited particles) filling the column was carefully extracted and divided into eight sections according to the transducers positions in order to measure the amount of retained particles along the medium. The mass of the deposited particles in each section was then determined according to the procedure described in Alem *et al.* [2]. For each section, an average value of retention defined as the ratio between the volume of the retained particles in the section and the volume of the section, was calculated. Retention profile along the porous medium was then determined.

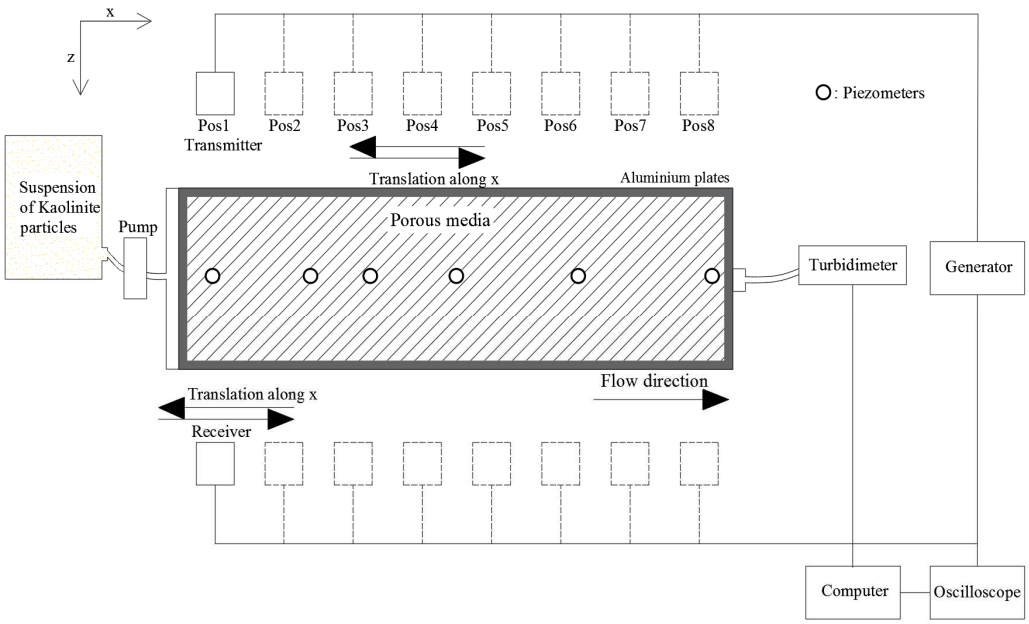

Fig. 2. Experimental setup for acoustic and mechanical analyses of the clogging phenomenon. The column containing the medium is fixed and the transducers move along the horizontal x axis (eight positions are shown corresponding to different layers having roughly the same properties in the clogged medium). The distance between the two transducers is 36 cm.

3. Evaluation of particle deposition using the destructive method

3.1. Restitution curves and deposition profiles

Figure 3 shows the experimental breakthrough curves (BTCs) of the injected SusP and the retention profiles in the three porous media. It also shows comparison between experimental and computed data according to the analytical solutions (Eqs. 15 and 16). The BTCs (Fig. 3a) are represented by the relative concentration C/C_0 as a function of time (C is the outlet concentration and C_0 the constant inlet concentration). For the three media, the rate of recovered particles increases rapidly to reach a plateau after an injected volume of about two pore volumes (initial stage) and then increases quasi-linearly up to the end of experiment (transient stage). Evolution of C/C_0 in the transient stage indicates a gradual deterioration in the filtration capacity of the medium with time. Indeed, during filtration, SP removal decreases because the deposited particles occupied the limited number of retention sites in the porous media. Comparing the BTCs of the three media, the value of the relative concentration C/C_0 at the plateau is lowest for ROBU (14%), slightly larger for Tobermorite (14.5%) and very large for GB (32%). Robu and Tobermorite are the most filtering of the three media. This suggests that suspended particles accessed a part of retention sites of the microporosity, namely for Robu, increasing their probability of capture. This results in a higher trapping of suspended particles in the microporosity, explaining higher filtration capabilities of the two DPP media. The rate of the increase of C/C_0 with time is highest for SPP medium and virtually similar and very low for the two DPP media. That is due to the rapid saturation of retention sites, fewer in SPP medium than in both DPP media, leading to rapid clogging of SPP medium (the presence of microporosity in Robu and Tobermorite provides additional retention sites delaying the clogging). Thus, the filtration capacity of these two media degrades more slowly during filtration than that of glass beads.

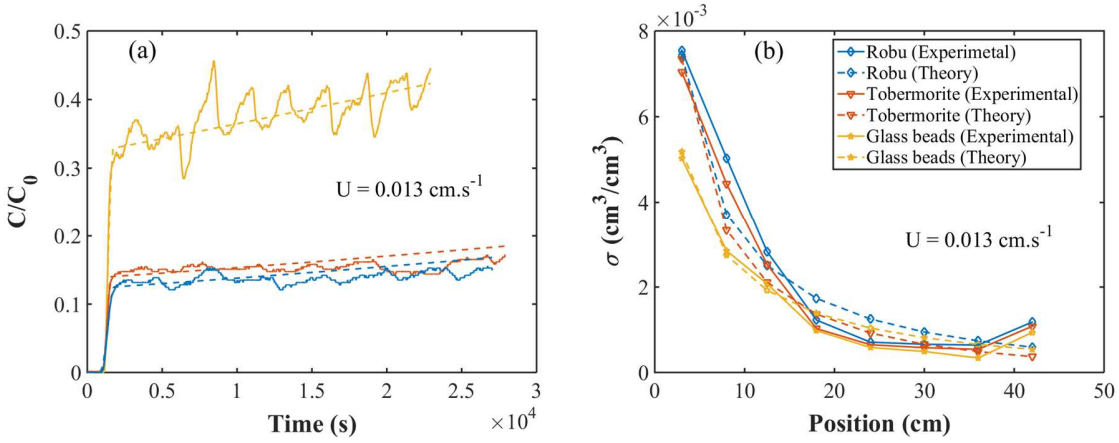

Fig. 3. Experimental and simulated (a) breakthrough curves (BTCs), and (b) deposition profiles.

Figure 3b shows that particle deposition is non-uniformly distributed in the pore space. Indeed, the deposition is more important in the first centimeters near the entrance of the medium and decreases with depth. The comparison of the retention profiles between the three porous media shows that retention at a fixed depth is globally highest for Robu, sligtly lower for Tobermorite, and is the weakest for GB. This observation is more marked for the first ten centimeters of the medium where the deposition is more important. Despite the high total porosity (70%) and microporosity (31%) of Tobermorite, the small sizes of a large part of micropores in Tobermorite grains suggests less access of suspended particles to these pores leading to less probability of their capture. However, for Robu, the sizes of the micropores are large enough that the particles in suspension can access a large part of these pores which explains the higher values of deposition.

Let σ be the local retention defined as the volume of particles deposited per unit volume of the porous medium, U the Darcy velocity, C the concentration of suspended particles, z the axial distance along the column, t the time, and $t_c = t - z\phi / U$ the time corrected for the initial filtration at different positions. Neglecting diffusion and assuming a small rate of change in porosity, the process of capture of injected SusP into a porous medium can be described, for one dimensional flow, by a mass conservation and rate equations for the particles in its simplest form as

$$\frac{\partial \sigma}{\partial t_c} + U \frac{\partial C}{\partial z} = 0 , \qquad \frac{\partial \sigma}{\partial t_c} = U \lambda_0 \psi C \tag{12}$$

λ_0 is the first order filtration coefficient of the medium. ψ is a dimensionless retention function that accounts for time and depth dependent deposition, it is expressed as:

$$\psi = \zeta^{-\beta} \exp(\alpha t) \tag{13}$$

Where $\zeta(z) = 1 + z/d_{50}$ with d_{50} the median grain size of the porous medium. The empirical parameter β controls the shape of the spatial distribution of retained particles and accounts for the depth dependence of filtration coefficient. The term $\zeta^{-\beta}$ describes depth-dependent retention (a decreasing rate of retention with depth). This term equals *1* for $\beta = 0$ and an exponential distribution of retained particles with depth is predicted similar to conventional filtration theory. On the other hand, for $\beta > 0$, the retention profile exhibits an hyperexponential shape with a higher deposition rate close to the porous medium inlet. In this study, $\beta = 0.432$ was retained based on Bradford *et al*. [26]. The term $\exp(\alpha t)$ with $\alpha < 0$ accounts for time-dependent retention. It explains filling phenomenon of retention sites and implies a decrease of retention capacity with time. Substituting the second equation of Eq. (12) into the first equation of Eq. (12), a linear first order solution is derived as follows:

$$\lambda_0 \psi C + \frac{\partial C}{\partial z} = 0 \tag{14}$$

Using the boundary condition $C(0, t_c) = C_0$, the following solution of Eq. (14) is found :

$$C(z, t_c) = C_0 e^{-\Lambda_0 d_{50} D_0 \exp(\alpha t_c)} \tag{15}$$

where $\Lambda_0 = \lambda_0 / (1-\beta)$ and $D_0 = \left[\zeta^{1-\beta} - 1\right]$. Inserting the expression for C (Eq. (15)) in the second equation of Eq. (12), a simple linear first order differential equation is obtained.

Considering the initial condition $\sigma(z, 0) = 0$, the solution of this differential equation is obtained.

$$\sigma(z, t_c) = \frac{U(1-\beta)}{\alpha d_{50}} \frac{\zeta^{-\beta}}{D_0} \left[e^{-\Lambda_0 d_{50} D_0} - e^{-\Lambda_0 d_{50} D_0 \exp(\alpha t_c)} \right] \tag{16}$$

In Eqs. 15 and 16, the initial stage (first two pore volumes), where the rate of recovered particles increases from 0 to the plateau, has been neglected. Eqs. 15 and 16 are used to evaluate the evolution with time of the restitution at the outlet of the medium, and the deposition profile in the porous medium at the end of each injection test.

The comparison between experimental and calculated results of the restitution (Fig. 3a) and the deposition profiles (Fig. 3b) shows globally good agreement, suggesting that the model, despite its simplicity, provides a satisfactory prediction of particle removal by the SPP or the DPP media.

For each medium, an average initial filtration coefficient $\overline{\lambda_0}$ is calculated

$$\overline{\lambda_0} = \frac{\lambda_0}{L}\int_0^L \left(1+\frac{z}{d_{50}}\right)^{-\beta} dz = \frac{\lambda_0 d_{50}}{L}\left[\frac{\zeta^{1-\beta}(L)-1}{1-\beta}\right] \quad (17)$$

$\overline{\lambda_0}$ (in cm^{-1}) is the highest for Robu (0.042), slightly lower for Tobermorite (0.040), and is the weakest for GB medium (0.022). This confirms that the filtration capacity, thanks to additional retention sites available in microporosity, is larger for the DPP media (Robu and Tobermorite respectively) than the SPP medium (GB). Values of the coefficient α (in s^{-1}) indicate a rate of the filtration capacity drop with time in the decreasing order GB (-1.5×10^{-5}), Tobermorite (-5.1×10^{-6}) and Robu (-5.1×10^{-6}). Knowing at any time the deposition profile in the medium is very interesting because the evolution of the permeability (not investigated in this paper) depends not only on the mass of deposited particles but especially on the deposition profile in the medium (Alem *et al.* [2]). This result confirms the availability of more capture sites in the DPP medium and the accessibility of SusP to the microporosity of this medium.

4. Ultrasonic detection of particle deposition

4.1. Temporal signals and phase velocities

The study of the acoustic wave transmission through porous media allows tracing the evolution of temporal signals in a bandwidth determined according to the central frequency of the transducer (Fig. 4). The translation of the transducers along the horizontal axis makes it possible to record the acoustic signals in eight different positions along the column. The materials are not quite arranged in the same way along the column (manual filling), thus the initial signals received on each position are slightly different, which turns out to be normal considering that the positioning of grains is done randomly. Figs. (4a and 4b) shows the change of the temporal signals amplitude (in Volts) for Robu (the changes for the two other materials are similar) before and after 2 hours and 7 hours of injection (for better readability only signals of positions 1 and 8 are shown). One notes that the signal amplitude decreases after injection, for all positions. The

deposition of particles in the medium causes absorption implying energy losses and therefore a decrease in amplitude. However this diminution is less pronounced for position 8 (Fig. 4b), a consequence of the fact that particles are deposited less and less when approaching the outlet of the column. The spectral representation of the impulse responses are given in Figs. (4c and 4d). From these curves, the attenuation of the signal transmitted through the turbid medium (after injection), describing the energy loss caused by the particle deposition, was determined.

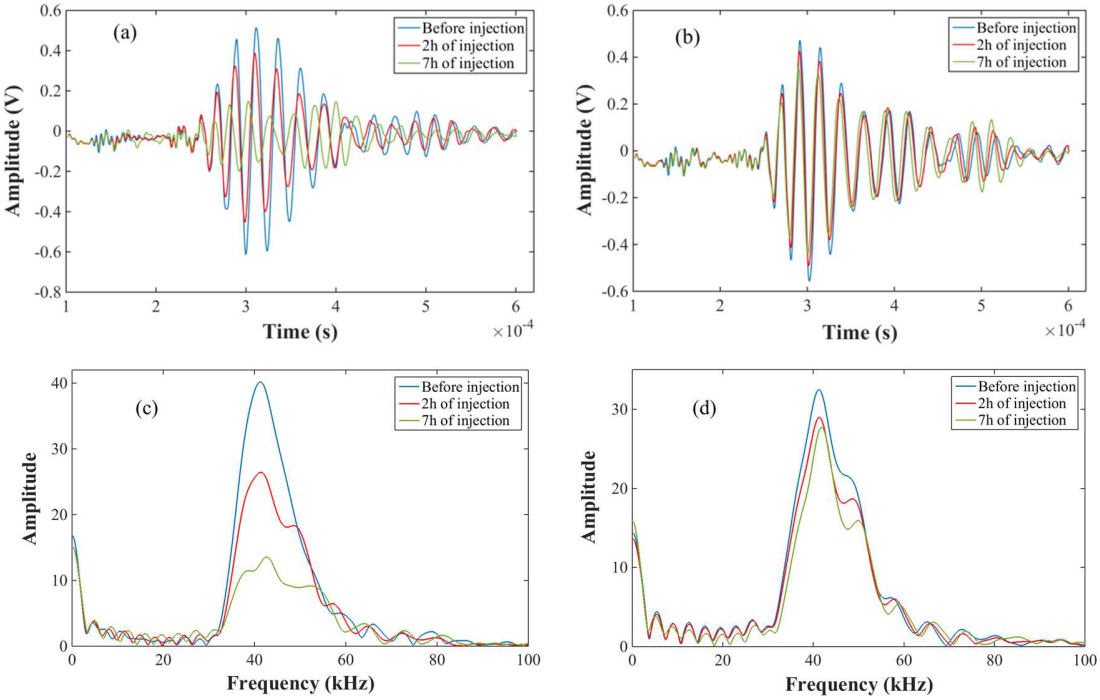

Fig. 4. Temporal signals of Robu for position 1 (a) and for position 8 (b). Spectral representation of the impulse response for position 1 (c) and for position 8 (d), before and during injection.

The pulse observed on the temporal signals corresponds to the arrival of the first longitudinal wave in the medium. The arrival time of this wave varies after particle deposition and an offset of the temporal signals towards the low frequency is noticed. Indeed, after injection, some porous spaces are occupied by the particles forming a solid skeleton, thus the difference in the inertia forces between the fluid and the solid part is less important, which explains a faster arrival of the pulse. Following this, and knowing the distance between the two transducers which is equal to 36 cm, as well as the velocity of the wave propagation in water and based on the flight time, the propagation velocity of the fast longitudinal wave in the three materials are determined in each

position of the column as a function of time, (Figs. 5a, 5b and 5c). For a better readability of the results, only four positions are presented in the following results. For the three media, one observes an increase in phase velocity with time injection for all positions, which can be explained by an important deposition with time. At a fixed time of injection, a decrease in velocity is noticed when going from the first position to the eighth one (from the entrance to the exit of the column), explained by a decrease of the accumulate deposition with depth as it was shown in Fig. 3.

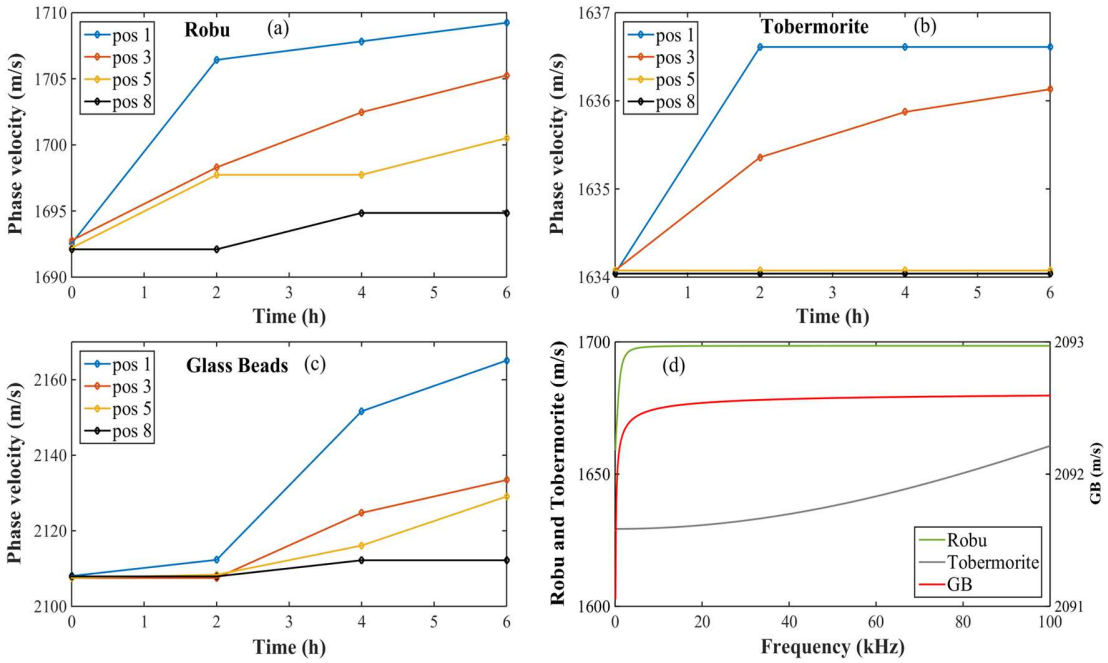

Fig. 5. Measured phase velocities of Robu (a), Tobermorite (b) and GB (c) before (t =0 hour) and during injection for four positions. Theoretical phase velocities (d) of Robu and Tobermorite (left axis) and GB (right axis).

In order to compare experimental results to the theoretical ones, phase velocities corresponding to the propagation of the first longitudinal wave in the three materials were calculated; their evolutions with the frequency are presented in Fig. 5d. The comparison was made between the theoretical values taken in the domain not far from the central frequency (Fig. 5d) and the experimental ones (Figs. 5a, 5b and 5c) taken at t = 0 (before injection). One observes that the velocity increases with frequency abruptly up to about 5 kHz and remains quasi-constant

for GB as well as for Robu. At t = 0, the values are identical to the experimental values with a difference of a few m/s. For Tobermorite, the phase velocity varies exponentially and continues to increase with frequency; its value for the central frequency ($V \approx 1635 m/s$) confirms that obtained experimentally before injection (Fig. 5b).

4.2. Energy and wave attenuation

The temporal signals transmitted through the studied materials have been interpreted in order to model the clogging phenomenon. The signals in this case indicate the energy by which the waves have been transmitted through the porous media. A change of these signals after particle deposition is visualized (Fig. 4) and it is explained by a loss of energy transmitted through the medium during injection. From that, one introduces the signal energy which is frequently used in signal processing $E = \int |x(t)|^2 dt$ where $_x$ (in volts) is the realized measurement modulus squared (in the present case, the amplitude of transmitted signal). As previously specified, the signals at each position along the horizontal axis of the model differ slightly because of the manual filling of the material in the column. For this reason, the calculation of the energy has been made with reference to the signal obtained before injection (clean medium). Therefore the evaluation of the deposition corresponds to the difference of the energies before (E_b) and after (E_a) each hour of particle injection $\Delta E = E_b - E_a$. Figs. (6a and 6b) show the variation of ΔE with the x-position for Robu and GB (Tobermorite is not presented here for simplification). The values of ΔE at the entrance are very important compared to other positions. At the outlet, the difference in energy becomes almost zero, this is directly related to the curves of the deposition profiles (Fig. 3b). Comparing the two media, the evolution of ΔE with time is more pronounced in Robu because of the presence of micropores which are accessible to the particles. We can, therefore, confirm that particles penetrate in both macropores and micropores.

Another way to highlight the particle deposition influence on the acoustic properties is to consider the attenuation of the transmitted wave based on the well-known Beer's law $r = D^{-1} \ln(A_0 / A_x)$ where $_r$ is the attenuation, D the distance between the two transducers, A_0 the reference signal amplitude taken here before injection at t = 0 and A_x the signal amplitude

during injection. These amplitudes are determined from the spectrum of the signal obtained by calculating the Fast Fourier Transform (FFT) (Figs. 4c and 4d).

The attenuation of ultrasonic waves in porous media is caused by viscous friction due to the relative motion of the fluid to the frame (in the frequency range considered here, the other possible source of attenuation, the scattering due to the contact between the grains, can be neglected) between the fluid and the solid. One presents the attenuation of the first longitudinal wave with time (Figs. 6c and 6d) for Robu and GB. There is an increase of the attenuation with time and a drop in space (from pos1 to pos8). The presence of particles in the pores generates a larger differential movement between the solid and the fluid phases, causing an increasing dissipation of energy and thus an augmentation in attenuation with time. In position 1, and as previously explained, a large part of particles that propagate in the medium are trapped in the first centimeters of the medium. This is why a very pronounced increase of attenuation is observed there. From the third position, this variation becomes less important, especially for the first hours of injection which the attenuation is almost constant.

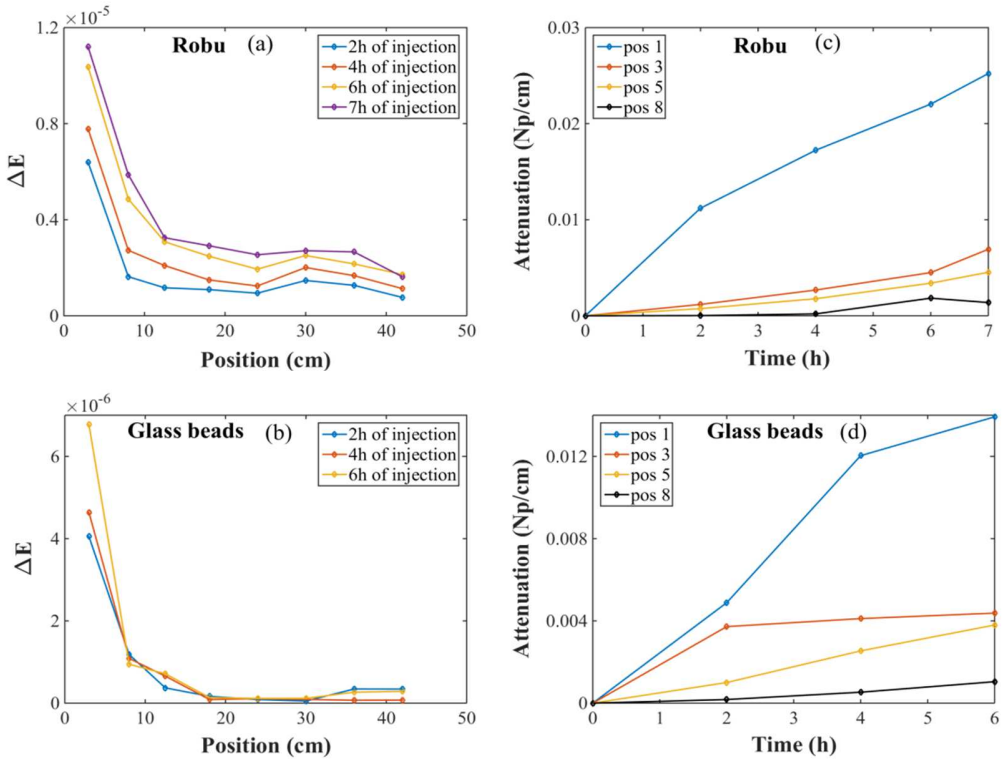

Fig. 6. Variation of energy for transmitted signals: Robu (a) and GB (b). Attenuation profiles for transmitted signals: Robu (c) and GB (d), after particle injection, for four positions.

5. Comparison between ultrasonic and destructive evaluations

In order to find a link between particle deposition and energy variation of the transmitted signal, we represent in Fig. 7, the spatial variation with depth of the deposition and of ΔE for the three materials. The accumulation of particles in the entrance of the column is confirmed by a great change in ΔE after injection. The higher the change in ΔE, the smaller the distance from the entrance. Near the outlet of the column, ΔE continues to vary in the same way as the deposition profile for the three materials, however, from the fourth position approximately (at 20 cm), the variation becomes very slight compared to the entrance. One observes that ΔE is very low in Tobermorite despite a high deposition (the deposition affects very few its acoustic characteristics).

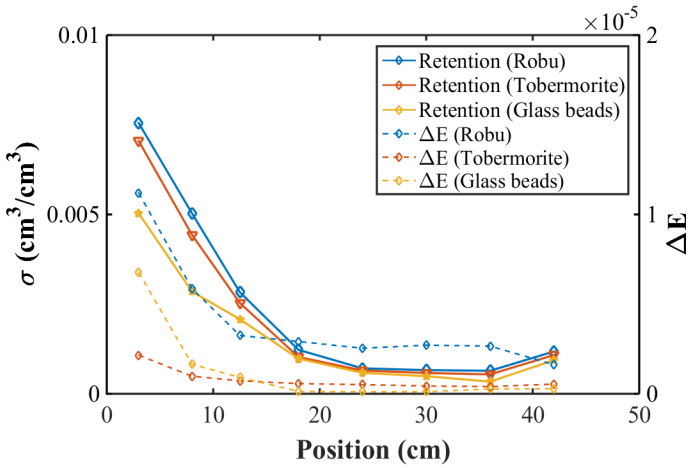

Fig. 7. Comparison between deposition profiles (left axis) and energy variation profiles (right axis) along the horizontal x axis for the three materials.

Based on these representations and knowing that the porosity decreases with the deposition, one have established links, on the one hand, between the phase velocity of the first longitudinal wave and the total porosity during injection, and on the other hand, between ΔE of the transmitted signal and porosity variation. Figs. (8a and 8b) show these links respectively for Robu, Tobermorite and GB. A linear relation (Fig. 8 (a)) between the velocity of the first longitudinal wave and the total porosity is obtained, for the three porous media. The velocity decreases linearly with increasing porosity. The variation of the phase velocity is mainly due to the change occurring for the porosity of the medium as consequence of particle deposition

explained by lower ultrasonic velocity and elastic constant of the deposition material compared to the porous medium. Since the retention is very high in the first positions, a decrease in porosity occurs. Consequently, the medium tends to an elastic one. This is why one observes higher values of the velocity after injection (especially in the entrance). The slope of the linear relation between velocity and porosity is a very good indicator of the rate of medium degradability due to deposition. This coefficient is very low for the two DPP media, but it is very high for the SPP medium. As previously underlined, the presence of microporosity in the DPP media provides additional sites for the capture of suspended particles. The decrease of the velocity with porosity was also observed by Kohout [3]. In his work, he studied several porous media with different porosities limited to 33%, contrary to our study where we reached porosities up to 70%.

The variation of the acoustic energy of the transmitted signal through the medium is simulated very satisfactorily by the following empirical relation $\Delta E = p e^{q\Delta\phi}$ where $\Delta\phi$ is the variation of the total porosity at time t, and p , q the calibration coefficients that depend on the characteristics of the medium. The coefficient q is an indicator of the degradation rate of the acoustic characteristics by the deposition. It is also a good indicator of the clogging velocity of the porous medium. The values of q are 2.036, 3.023 and 7.930 for Robu, Tobermorite and GB respectively, which means that the clogging in the SPP GB is faster than that in Tobermorite and in Robu. These measurements can also provide information about the evolution of the characteristics of the medium, and thus in this study of clogging. The ultrasonic method for determining the porosity of solid samples appears promising in the zone of the tested porosities. After proper calibration, it should be possible to use it to determine the porosity of any porous medium. The measurement is rapid and the method is non-destructive.

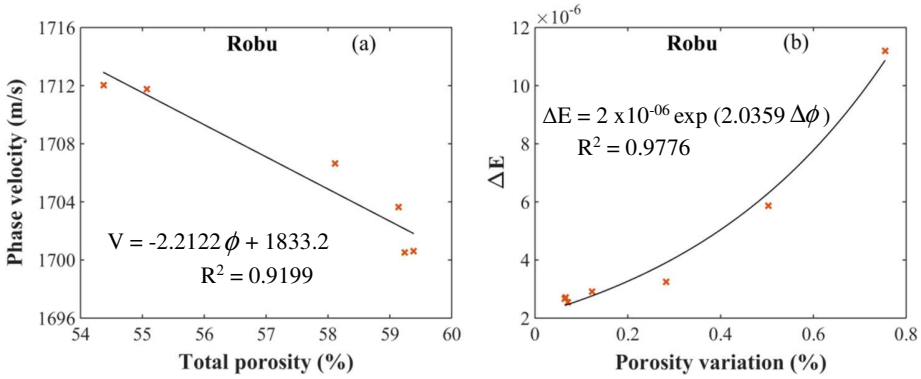

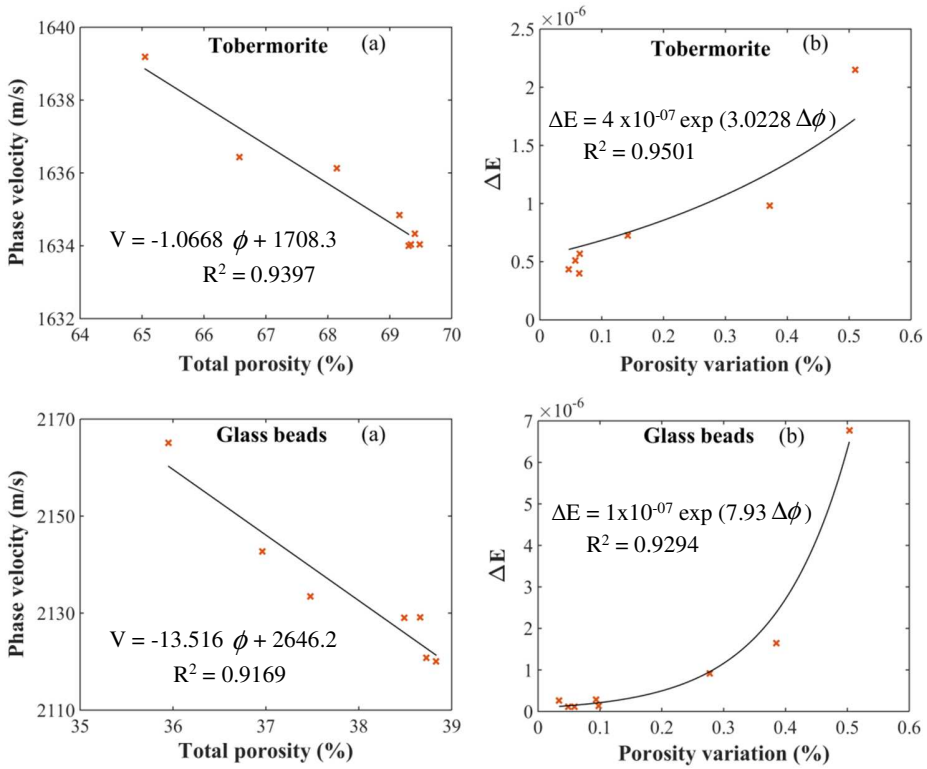

Fig. 8. Phase velocity versus total porosity (a) and variation of energy for transmitted signals versus porosity variation (b), for Robu, Tobermorite and GB after particle injections (t = 6 hours).

6. Conclusions

The clogging phenomenon in porous media is quite complicated by the different processes that describe it. Deposition mainly affects porosity and permeability, which are the most important parameters in porous media, particularly in water retention structures. The increase in deposition with time causes a drop in permeability which can have adverse consequences on the proper functioning of a medium.

Several parameters can be involved in the fine particles deposition in a saturated porous medium. The comparison of three different materials (two of them with double porosity and the third one with single porosity) made it possible to deduce the great importance of the medium structure in the particle deposition. The retention capacity of the medium depends closely on the tortuosity and the size (length and diameter) of the micropores (for Tobermorite, despite a very

high porosity, this capacity is less important compared to Robu which contains larger and deeper micropores).

Concerning the clogging, despite the uncertainties in the measurements a relation is observed between the destructive evaluation and the non destructive ultrasonic detection based on wave transmission through the medium. The variation of acoustic properties (phase velocity, transmitted signal energy and wave attenuation) with the deposition has been presented. Indeed, the curves of the attenuation and the energy variation are directly related to the deposition profile. The fast longitudinal velocity estimated by the flight time varies in time and in space as well with the clogging. A linear variation of the velocity with the total porosity obtained after injection is given, which is expected because the velocity depends strongly on the medium density, and therefore on its porosity. We have also observed an exponential dependence of the signal energy variation with the porosity variation due to deposition. From these results, one deduces the sensitivity of acoustic methods to the phenomenon of clogging.

A phenomenon not taken into account in our experiments is that of multiple scattering between beads which would result from the use of high frequencies (we took care to avoid this by choosing fairly low frequencies). During the flow of the turbid solution, some particles can be deposited on the grain surfaces; therefore, the multiple scattering could be influenced by the change in the cross section of the scatters due to the accumulation of the particles on their surfaces. In addition to the attenuation caused by this multiple scattering, another source of attenuation is due to the conversion of fast waves into slow waves in the matrix (seat of the micropores) during the flow (which is no longer of the Poiseuille type) induced by the passage of these waves [27] for example. All these phenomena gain importance at high frequencies and deserve to be examined closely during more detailed experimental studies.

Appendix

The elements t_{ij} $(i, j = 1,2,3)$ in the dispersion equation, Eq. (10), are

$$t_{11} = -\ell^2 \left[K_u + \frac{4}{3}\mu + K_u \left(B^{(1)} \nu^{(1)} \phi^{(1)} + B^{(2)} \nu^{(2)} \phi^{(2)} \right) \right] + i\omega \left(b_{12} + b_{13} \right) + \omega^2 \rho_{11} \ ;$$

$$t_{12} = -\ell^2 K_u B^{(1)} \nu^{(1)} \phi^{(1)} - i\omega b_{12} + \omega^2 \rho_{12} \ ; \ t_{13} = -\ell^2 K_u B^{(2)} \nu^{(2)} \phi^{(2)} - i\omega b_{13} + \omega^2 \rho_{13} \ ;$$

$$t_{21} = -\ell^2 \left(C_{21} + C_{22} \nu^{(1)} \phi^{(1)} + C_{23} \nu^{(2)} \phi^{(2)} \right) - i\omega b_{12} + \omega^2 \rho_{12} \ ; \ t_{22} = \ell^2 C_{22} \nu^{(1)} \phi^{(1)} + i\omega b_{12} + \omega^2 \rho_{22} \ ;$$

$t_{23} = \ell^2 C_{23} \nu^{(2)} \phi^{(2)} + \omega^2 \rho_{23}$;

$t_{31} = -\ell^2 \left(C_{31} + C_{23} \nu^{(1)} \phi^{(1)} + C_{33} \nu^{(2)} \phi^{(2)} \right) - i\omega b_{13} + \omega^2 \rho_{13}$;

$t_{32} = \ell^2 C_{23} \nu^{(1)} \phi^{(1)} + \omega^2 \rho_{23}$; $t_{33} = \ell^2 C_{33} \nu^{(2)} \phi^{(2)} + i\omega b_{13} + \omega^2 \rho_{33}$.

The elements q_{ij} ($i, j = 1, 2, 3$) in the dispersion equation, Eq. (11), are

$q_{11} = -\mu\ell^2 + i\omega\left(b_{12} + b_{13}\right) + \rho_{11}\omega^2$; $q_{12} = q_{21} = \rho_{12}\omega^2 - i\omega b_{12}$;

$q_{13} = q_{31} = \rho_{13}\omega^2 - i\omega b_{13}$; $q_{23} = q_{32} = \rho_{23}\omega^2 - i\omega b_{23} \left(\equiv 0, \text{if } \rho_{23} = 0 \text{ and } b_{23} = 0\right)$;

$q_{22} = \rho_{22}\omega^2 + i\omega b_{12}$; $q_{33} = \rho_{33}\omega^2 + i\omega b_{13}$.

The expression for the mass densities ρ_{ij} ($i, j = 1, 2, 3$) and for the drag coefficients b_{ij} ($i, j = 1, 2, 3$) can be found in Ref. [12]. The mass densities ρ_{ij} depend on the porosities and mass density of the fluid ρ_f and solid ρ_s but also on the three types of tortuosity: $\tau^{(1)}$ (micropores), $\tau^{(2)}$ (macropores) and τ (global). The drag coefficients b_{ij} depend on the fluid viscosity, the porosities and the permeabilities. For the computation of the b_{ij} s, we follow Berryman and Wang who showed that in wave propagation studies, the permeabilities accounting for the coupling between micropores and macropores can be neglected, resulting in simplified formulas.

References

[1] Moghadasi J, Müller-Steinhagen H, Jamialahmadi M, Sharif A. (2004). Model study on the kinetics of oil field formation damage due to salt precipitation from injection. *J. Pet. Sci. Eng*, 43 (3–4); p. 201 – 217.

[2] Alem A, Elkawafi A, Ahfir N, Wang H. (2013). Filtration of kaolinite particles in a saturated porous medium: hydrodynamic effects. *Hydrogeology Journal*, 21, p. 573 – 586.

[3] Kohout T, Karlqvist R, Eskelinen J, Hortling A, Pesonen LJ, Hæggström E. (2013). Ultrasonic Determination of Porosity in Homogeneous Ceramic Samples. *Geophysica*, 49 (1–2); p. 25 – 32.

[4] Allard J, Castagnède B, Henry M, Lauriks W. (1994). Evaluation of tortuosity in acoustic porous materials saturated by air. *Rev. Sci. Instrum*, 65; p. 754 – 755.

[5] Melon M, Castagnède B. (1995). Correlation between tortuosity and transmission coefficient of porous media at high frequency. *J. Acoust. Soc. Am*, 98; p. 1228 – 1230.
[6] Fellah Z, Fellah M, Mitri F, Sebaa N, Depollier C, Lauriks W. (2007). Measuring permeability of porous materials at low frequency range via acoustic transmitted waves, *Rev. Sci. Instrum*, 78; p. 114902-1 – 114902-10.
[7] Biot MA. (1956). Theory of propagation of elastic waves in a fluid-saturated porous solid. I. Low-frequency range. *J. Acoust. Soc. Am*, 28; p. 168 – 178.
[8] Jocker J, Smeulders D. (2009). Ultrasonic measurements on poroelastic slabs: Determination of reflection and transmission coefficients and processing for Biot input parameters. *Ultrasonics*, 49; p. 319 – 330.
[9] Lauriks W, Boeckx L, Leclaire P. (2005, Dec). Characterization of porous acoustic materials. *SAPEM Symposium on the Acoustics of Poro-Elastic Materials (Lyon, France).* <hal-01329870>.
[10] Warren JE, Root PJ. (1963). The behavior of naturally fractured reservoirs. *J. Soc. Pet. Eng*, 3; p. 245 – 255.
[11] Wilson RK, Aifantis EC. (1984). A double porosity model for acoustic wave propagation in fractured porous rock. *Int. J. Eng. Sci*, 22; p. 1209 – 1217.
[12] Berryman JG, Wang HF. (2000). Elastic wave propagation and attenuation in a double-porosity dual-permeability medium. *Int. J. Rock Mech. Min. Sci*, 37; p. 63 – 78.
[13] Dai ZJ, Kuang ZB, Zhao SX. (2006 b). Reflection and transmission of elastic waves from the interface of fluid- saturated porous solid and a double porosity solid. *Transp. Porous Med*, 65; p. 237 – 264.
[14] Kachkouch F, Franklin H, Tinel A. (2018). Reflection and transmission characteristics of a layer obeying the two pressure field poroelastic phenomenological model of Berryman and Wang. *Ultrasonics*, 87; p. 71 – 81.
[15] Bai R, Tinel A, Alem A, Franklin H, Wang H. (2016). Estimating frame bulk and shear moduli of two double porosity layers by ultrasound transmission. *Ultrasonics*, 70; p. 211 – 220.
[16] Arbogast T, Douglas J, and Hornung U. (1990). Derivation of the double porosity model of single phase flow via homogenization theory. *SIAM J. Math. Anal*, 21; p. 823 – 836.
[17] Auriault JL, Boutin C. (1993). Deformable porous media with double porosity. III. Acoustics. *transp. Por. Media*, 14; p. 143 – 162.

[18] Chotiros NP, Isakson MJ. (2014). Shear wave attenuation and micro-fluidics in water saturated sands and glass beads. *J. Acoust. Soc. Am*, 135 (6); p. 3264 – 3279.

[19] Kimura M. (2008). Experimental validation and applications of a modified gap stiffness model for granular marine sediments. *J. Acoust. Soc. Am*, 123; p. 2542 – 2552.

[20] Bai R, Alem A, Franklin H, Tinel A, Wang H, Kachkouch F, Taibi S, Bizet L. (2018). Ultrasonic characterization of particle retention by a double porosity medium, Environmental Technology, 40: 9; p. 1166 – 1177. DOI: 10.1080/09593330.2017.1417494.

[21] Chrysikopoulos CV, Syngouna VI. (2014). Effect of Gravity on Colloid Transport through Water-Saturated Columns Packed with Glass Beads: Modeling and Experiments. *Environ. Sci. Technol*, 48; p. 6805 – 6813. dx.doi.org/10.1021/es501295n.

[22] Kimura M. (2006). Frame bulk modulus of porous granular marine sediments, *The Journal of the Acoustical Society of America*, 120; 699. DOI: 10.1121/1.2211427.

[23] Stoll RD, Kan TK. (1981). Reflection of acoustic waves at a water-sediment interface. *J. Acoust. Soc. Am*, 70 (1); 149. https://doi.org/10.1121/1.386692

[24] Plona TJ. (1980). Observation of a second bulk compressional wave in a porous medium at ultrasonic frequencies. *Appl. Phys. Lett*, 36, 259.

[25] Dai ZJ, Kuang ZB. (2006). Reflection and transmission of elastic waves at the interface between an elastic solid and a double porosity medium. *International Journal of Rock Mechanics & Mining Sciences*, 43; p. 961 – 971.

[26] Bradford SA, Simunek J, Bettahar M, Van Genuchten MT, Yates SR. (2003). Modeling colloid attachment, straining, and exclusion in saturated porous media. *Environ. Sci. Technol*, 37, 10; p. 2242 – 2250.

[27] Müller TM, Gurevich B. (2005). A first-order statistical smoothing approximation for the coherent wave field in random porous media. *J. Acoust. Soc. Am*, 117; p. 1796 – 1805.